RSC Advances

PAPER

View Article Online
View Journal | View Issue

Cite this: *RSC Adv.*, 2023, **13**, 2256

SnO_2 mesoporous nanoparticle-based gas sensor for highly sensitive and low concentration formaldehyde detection†

Pengfei Liu, ‡[a] Jianbin Wang,‡[ce] Han Jin,[d] Meiying Ge,*[b] Fang Zhang,[b] Cheng Wang,[e] Yan Sun *[cf] and Ning Dai [c]

Received 25th October 2022
Accepted 1st January 2023

DOI: 10.1039/d2ra06745e

rsc.li/rsc-advances

Indoor air quality detection, especially formaldehyde (HCHO) detection, is of great importance in practical application. A key limitation of promoting gas-sensing devices is the lack of sensing materials with high sensing sensitivity and selectivity. In this study, SnO_2 mesoporous nanoparticles are fabricated by a facile hydrothermal route with a subsequent acid etching process. The prepared samples show high response toward HCHO (133.5, 222.8 for 100 ppm and 200 ppm HCHO, respectively) and short response/recovery time (15/22 s at 10 ppm). The excellent HCHO sensing performance benefits from the comprehensive regulation of the depletion region width, surface area and rich porosity, which is effective for the promotion of surface adsorption and catalyst activity. It is expected that the excellent sensing properties are promising for practical HCHO gas detection.

1. Introduction

Due to the advancement of urbanization and the transformation of human production and lifestyle, volatile organic compounds (VOCs), especially formaldehyde (HCHO) released by indoor, interior and automobile decoration materials have caused great harm to human health.[1–3] Therefore, the development of effective gas sensors for HCHO gas is becoming more and more urgent, which is of great significance for human health and environmental monitoring. So, the development of high sensitivity and selectivity sensing materials plays a key role for formaldehyde detection.

Metal oxide semiconductors (MOSs) are considered the most excellent sensing materials due to their high sensitivity, good stability, low cost, non-toxic and easy synthesis.[4–8] As one of the earliest gas sensitive materials, SnO_2 (n-type semiconductor) is the most actively research semiconductor material with excellent sensing performances. Up to now, considerable effort has been devoted to maximize the number of coordinative surface sites which would improve the adsorption and catalytic property,[9] of which synthesizing material with porous structure is the preferred approach to increase specific surface area.[10–12] Its major advantage is that mesoporous structure would have more active sites to improve the adsorption and exhibit good gas separation capability which might improve both the sensitivity and selectivity.[13,14] Another advantage is the defect engineering, through which the electronic structure of the sensing materials can be adjusted to improve the stability of the sensitive materials.[15] Wang *et al.* prepared mesoporous worm-like SnO_2 with pore diameter from 6 to 15 nm. The worm-like SnO_2 mesoporous nanostructures exhibit highly sensitive and selective to *n*-butanol.[16] The response of sensors based on mesoporous SnO_2 nanostructures reaches 435 with the *n*-butanol concentration 5 ppm. Some other researches show that mesoporous and porosity are vitally important for improving the sensitivity due to the high specific surface area and fast gas diffusion.[17–19]

Despite frequently reported progress mainly rely on the adjustability of mesoporous, the design of the mesopore diameter is still urgent as most reports have demonstrated mesopore by using polymers to adjust the aperture, such as poly(vinylpyrrolidone) or poly acrylonitrile.[20–22] The sacrificial template method can provide a framework for the final product and give it a specific size and pore structure. In this study, a sacrificial template synthetic route was developed to prepare SnO_2 mesoporous nanoparticles to produce abundant pore

[a]*School of Material Science and Engineering, Shanghai Jiao Tong University, No. 800 Dongchuan Road, Shanghai 200240, PR China*

[b]*National Engineering Research Center for Nanotechnology, 28 East Jiang Chuan Rd, Shanghai 200241, China. E-mail: meiyingge@163.com*

[c]*National Laboratory for Infrared Physics, Shanghai Institute of Technical Physics, Chinese Academy of Sciences, No. 500 Yutian Road, Shanghai 200083, PR China. E-mail: sunny@mail.sitp.ac.cn*

[d]*Institute of Micro-Nano Science and Technology, School of Electronic Information and Electrical Engineering, Shanghai Jiao Tong University, No. 800 Dongchuan Road, Shanghai 200240, P. R. China*

[e]*Institute of Biomedical Optics and Optometry, Key Laboratory of Medical Optical Technology and Instruments, Ministry of Education, University of Shanghai for Science and Technology, Shanghai 200093, China*

[f]*Research Center for Sensing Materials and Devices Zhejiang Lab, Hangzhou, Zhejiang, 311121, China*

† Electronic supplementary information (ESI) available. See DOI: https://doi.org/10.1039/d2ra06745e

‡ These authors contributed equally to the work.

structure with suitable particle size and high surface area. The prepared mesoporous nanoparticles not only show exhibited large specific surface area and rich porosity, with the pore diameter region was 2.7–4.5 nm, but also exhibit greatly enhanced sensitivity in detecting formaldehyde gas. The optical operating temperatures of corresponding sensor were determined to be 230 °C, the maximum response of sensors based on SnO_2 mesoporous nanoparticles was ~222.8 toward 200 ppm HCHO vapor. This study offers a new perspective for the design of sensing materials with nanosized of pores.

2. Experimental

2.1. Preparation of SnO_2/ZnO composites

All the chemicals were of analytical grade and were used as received without further purification. SnO_2/ZnO nanoparticle composites were successfully prepared by typical hydrothermal method. The SnO_2/ZnO nanocomposite samples were synthesized by 0.3692 g $SnCl_2 \cdot 2H_2O$, 0.0487 g $Zn(NO)_3 \cdot 6H_2O$ (Sn : Zn = 10 : 1) and 0.342 g thiourea. All of them were added into 70 mL ethylene glycol and magnetic stirred for 20 min at 30 °C to form a homogeneous solution. The solution was sealed in a stainless steel autoclave containing the Teflon inner tank. Heat the autoclave to 180 °C and keep for 24 hours, then cooled down to room temperature naturally. The as-obtained product was collected by centrifugation, then washed with ethanol and distilled water for several times. After that, the product was dried in an oven at 80 °C, and then calcined at 650 °C for 2 h at a heating rate of 5 °C min^{-1} and naturally cooled to room temperature. A sample of SnO_2/ZnO powder can be obtained.

2.2. SnO_2 mesoporous nanoparticles

The SnO_2/ZnO powder was put into 100 mL of nitric acid with the concentration of 5 wt% and the solution was sealed in a stainless steel autoclave containing the Teflon inner tank and kept at 150 °C for 8 hours, then cooled down to room temperature naturally. The as-obtained products were washed with deionized water and ethanol for several times, and dried at 70 °C. In this way, we will obtain the SnO_2 mesoporous nanoparticles after acid-etching process.

2.3. Characterization

The products were characterized through X-ray diffraction (XRD, Shimadzu XRD-6000, with high-intensity Cu, K radiation), scanning electron microscopy (SEM, Hitachi S-4800, operated at 5 kV), transmission electron microscopy (TEM, Hitachi H-800 with an accelerating voltage of 200 kV), and a high-resolution transmission electron microscope (HRTEM, JEM-2010, JEOL). The specific surface area and pore size distribution were determined through Brunauer–Emmett–Teller (BET) and Barrett–Joyner–Halenda (BJH) methods, respectively, using a Quantachrome Autosorb-1-C. The pore size distribution was calculated from the adsorption branch of the nitrogen adsorption–desorption isotherms using the Barrett–Joyner–Halenda (BJH) method. X-ray photoelectron spectroscopy (XPS) measurements were carried out under a Thermo ESCALAB 250 system using an Al-K 150 W non-monochromatized X-ray source and a hemispherical energy analyzer at a pass energy of 30 eV.

2.4. Sensor fabrication and testing

After cleaning, the ceramic tube is welded on the hexagonal base through platinum wire and nickel chromium heating wire. An appropriate amount of powder sample (about 0.1 g) is put into an agate mortar, and fully ground with an appropriate amount of distilled water (about 1 mL), until it becomes slurry. The powder is evenly smeared on the ceramic tube with a brush to form a uniform and dense gas-sensitive material film, and then placed in the air to dry naturally for 24 h. Then the electric heating wire is inserted into the ceramic center, and the gold electrode is welded to make the gas sensor. It was aged at 400 °C for 1 week to enhance its stability. We make five sensor devices for each sample.

At room temperature, the WS-30A intelligent gas sensing performance test equipment of Zhengzhou Weisheng Electronic Technology is used to calculate the resistance change of the gas sensing element through static side thermal measurement of the output voltage on the load resistor in series with the gas sensing element, so as to reflect the gas sensing characteristics of the sample. The sensor response was defined as $R = R_a/R_g$, where R_g and R_a were the electrical resistance of sensor in the testing gases and air, respectively.

3. Results and discussion

3.1. Structure and morphology characterization

The morphologies and crystallinities of the SnO_2 nanoparticles are characterized by SEM and TEM. The typical SEM image of the as-prepared products (Fig. 1a) revealed that the SnO_2 are irregular dispersed and composed by nanoparticles, and the heterointerface contact between nanoparticles can be envisaged. The TEM image of SnO_2 nanoparticles (Fig. 1b) shows an interconnected agglomeration with nanoparticles and the size of nanoparticle is ~21 ± 5 nm. Nano sized pores can be clearly observed in the nanoparticles, which shows that SnO_2 nanoparticles have mesoporous structures. Furthermore, the crystal orientation features were examined by HRTEM. As can be seen from Fig. 1c, mesoporous nanoparticles have clear lattice fringes with a crystal plane spacing of 0.327 nm, corresponding to the (110) crystal plane of tetragonal rutile SnO_2.[13] The change of crystal plane spacing compared with SnO_2 may be due to the increase of lattice strain ratio and transformation of crystal into mesoporous during the hydrothermal and acid-etching pore-creating process. Fig. 1d is the selected area electron diffraction (SAED) pattern of nanoparticles in Fig. 1b, which correspond to the SnO_2 crystal planes. A large number of diffraction spots in the SEAD pattern may be due to the good crystallinity of SnO_2 nanoparticles.

The crystal phase was characterized by XRD, and the results are shown in Fig. 2. All the diffraction peaks of both samples were matched with that of SnO_2 (JCPDS no. 41-1445) with tetragalite structure. The peak position and relative strength of

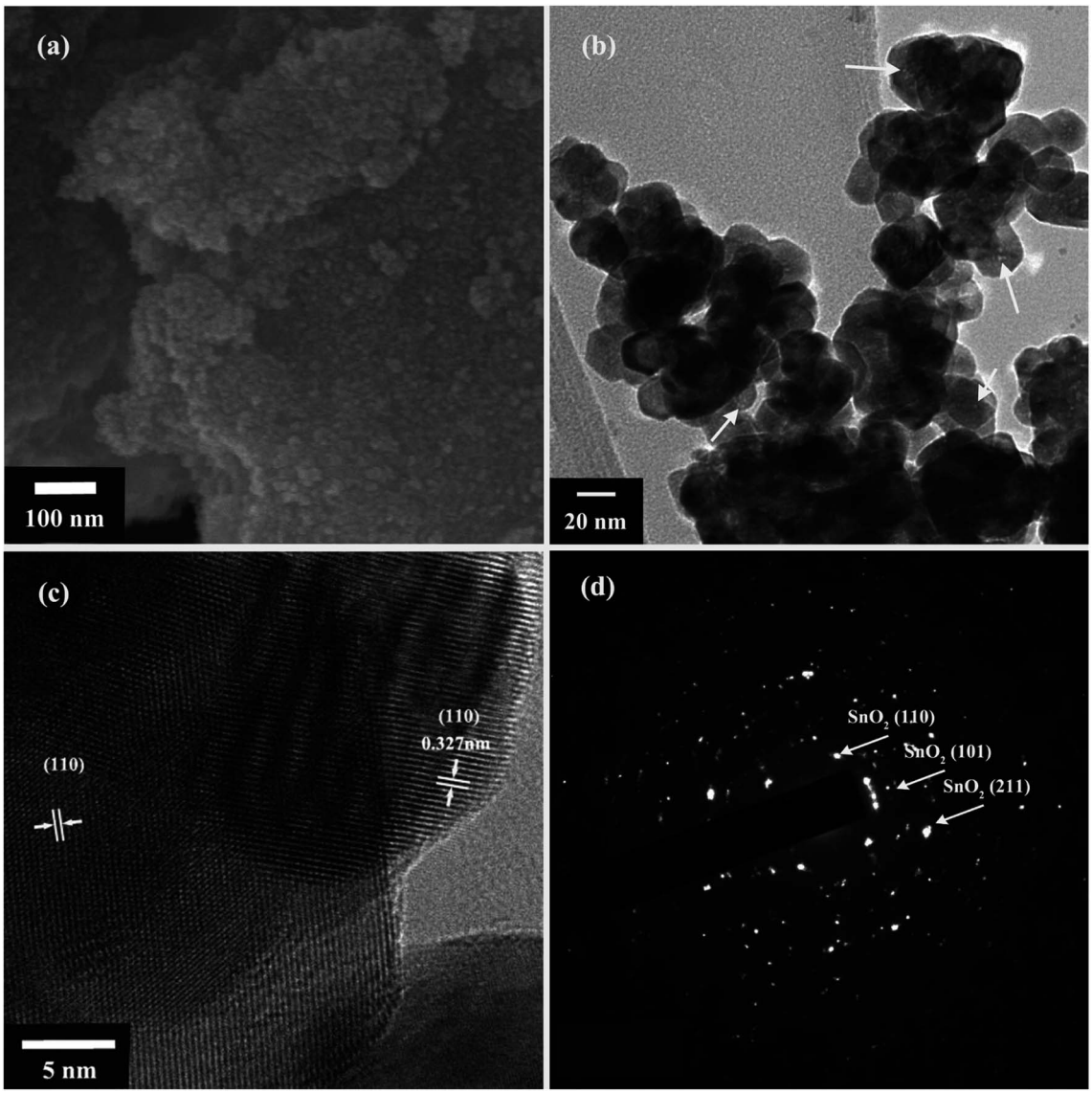

Fig. 1 (a) SEM image (b) TEM image (c) HRTEM image (d) SAED pattern of the mesoporous nanoparticles.

XRD patterns of mesoporous nanoparticles did not change compared with SnO_2 samples prepared by other methods.

The pore structure was measured by nitrogen adsorption–desorption isotherms and pore size distribution curves. As shown in Fig. 3a, there is an obvious adsorption hysteresis loop at the P/P_0 range of 0.45–0.90, which belongs to type IV nitrogen adsorption isotherm according to IUPAC classification.[16] The pore size distribution and specific surface area of the nanoparticles were obtained by using the Barrett–Joyner–Halenda measurement method, the nitrogen isotherm desorption curve and the multi-point Bunnell method (BET) measurement. The results show that a narrow peak appears at the pore size region is 4–7 nm, and a narrow peak appeared at the pore diameter of about 3.0 nm, and the pore diameter region was 2.7–4.5 nm. This indicates that a large number of pores around 3 nm are formed in SnO_2 matrix. In the relative pressure range of 0.05–0.3 (P/P_0), the BET specific surface area of nanoparticles is 97.29 m^2 g^{-1}. In general, the larger surface area and smaller grain size can supply more sites for O_2 adsorption, which could promote the activation of O_2 and HCHO.[13]

The XPS was used to detect the surface composition and chemical state of the as-prepared samples. The full spectrum of Fig. 4 a shows that O and Sn are the main elements in mesoporous nanoparticles, and Zn is removed from the nanoparticles with acid-etching process. Fig. 4b is the Sn 3d map of nanoparticles, and the peaks of Sn $3d_{5/2}$ and Sn $3d_{3/2}$ correspond to Sn^{4+} in SnO_2 mesoporous nanoparticles and are located at 487.2 eV and 495.6 eV, with an error of $\pm$0.7 eV.[22] As shown in Fig. 4c, the O 1s spectrum of nanoparticles has been divided into many peaks by Gaussian deconvolution. The atomic proportion of each corresponding chemical state is expressed by the area of each corresponding peak. The O 1s region of the nanoparticles with acid-etching was divided into three peaks, which represent lattice oxygen Sn–O, oxygen

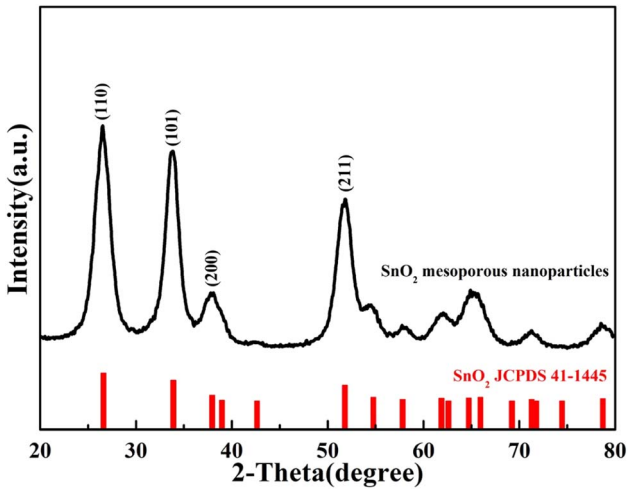

Fig. 2 XRD pattern of SnO_2 mesoporous nanoparticles.

vacancy, adsorbed oxygen O^- and O^{2-}, with corresponding ratios of 64.48%, 26.3% and 9.22%, respectively.[23] These peaks were located at 530.4 eV, 531.4 eV and 532.4 eV, respectively. The results show that the acid-etching can effectively remove lattice oxygen Zn–O and the void pores, which can adsorb more oxygen into adsorbed oxygen O^- and O^{2-}.

3.2. Gas sensing properties

The operating temperature is the key role for the sensing performance, so the sensing properties towards HCHO at different temperatures were measured to determine the optimum operation temperature. Fig. 5a shows the response value of five sensors of each sample to 100 ppm HCHO, within the error range of 5%, which shows that the sensor has a good reproducibility. As can be seen from Fig. 5a, the response value the mesoporous nanoparticles increased rapidly as the temperature arises. According to the surface-controlled model, chemisorption of oxygen on the surfaces of SnO_2 mesoporous nanoparticles transferred from a chemisorbed state to an ionized O^{x-} (such as O_2^-, O^-, O^{2-}).[9–12] These dissociative oxygen species lead to an electron–depletion layer on the surface of the sensing materials, which is dependent on the amount of ion sorption of O^{x-}. The maximum response of the sensor based on mesoporous nanoparticles sensor was attained up to 230 °C with a value of 133.5 for 100 ppm HCHO, because the concentration of active oxygen adsorbed on the sample surface has been maximized at the working temperature about 230 °C. As the temperature is higher than 230 °C, the adsorption of active oxygen ions on the sample surface is easy to desorb, so the response value of both samples decrease with the increase of temperature. Therefore, 230 °C was chosen as the testing temperature to proceed in the following experiments.

The selectivity of nanoparticles is tested, and the developed sensor was also investigated towards other interfering gases including methanol, acetone, ethanol, ammonia. As shown in Fig. 5b, the sensor based on SnO_2 mesoporous nanoparticles have a higher response value to HCHO, and the response is 222.8 at 200 ppm, while the response to other interfering gases is less than 35 with the 200 ppm of HCHO. There is no response for other gases such as NO_2, CO, toluene, methane. The response is higher in comparison to reported literature.[2,3,24]

The dynamic sensing properties of the sensors based on mesoporous nanoparticles toward HCHO gas in the concentration range of 0.5–200 ppm is examined at 230 °C as shown in Fig. 6a. The results show that sensors have fast response–recovery properties and good repeatability to HCHO gas. The response rises rapidly as the increase of HCHO concentration which indicates the good response recovery performance. The dynamic sensing properties of the sensors based on nanoparticles before acid etching was shown in Fig. S2.† At 200 ppm HCHO, the response value of SnO_2 mesoporous nanoparticles is 1.7 times of that before acid etching. Therefore, acid-etching can greatly improve the sensitivity of SnO_2 nanoparticles to

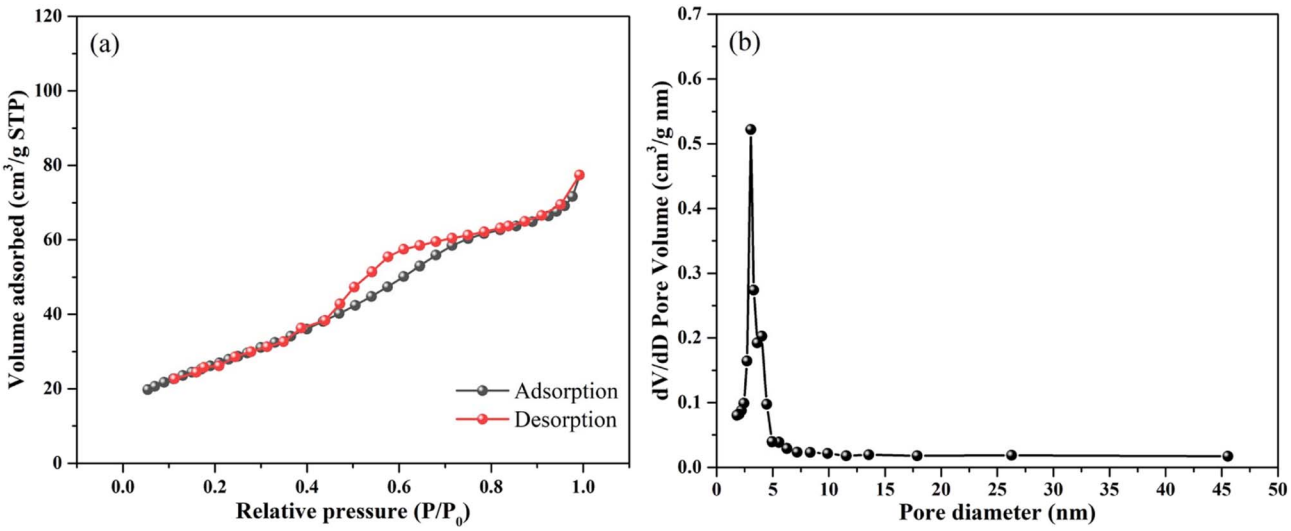

Fig. 3 (a) Nitrogen adsorption–desorption isotherm and (b) BJH pore size distribution plots of mesoporous nanoparticles.

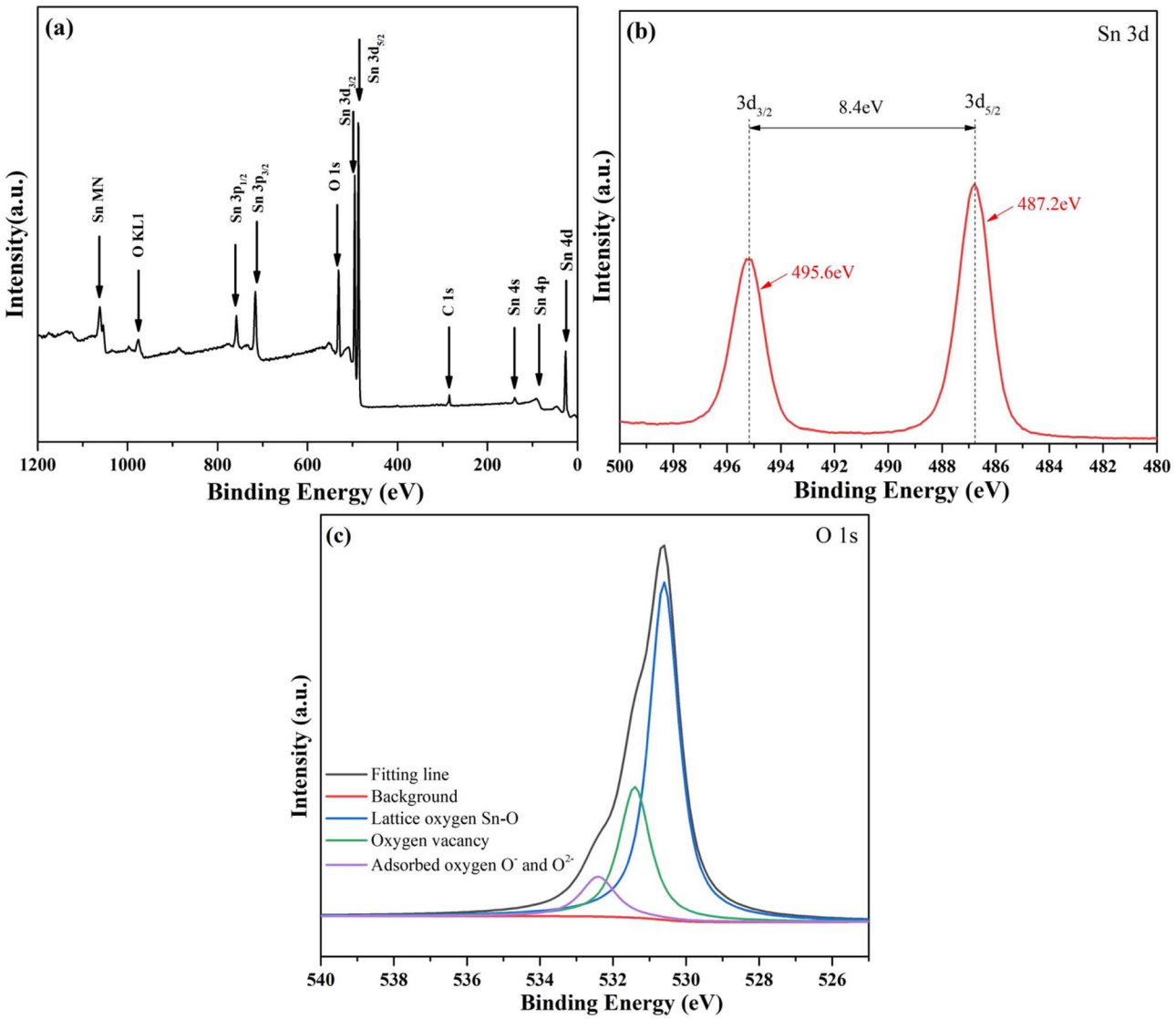

Fig. 4 (a) Survey spectra, (b) Sn 3d spectra, (c) O 1s spectra of mesoporous nanoparticles.

HCHO. Fig. 6b shows the image of the curve at 10 ppm. The response time and recover time are 15 s and 22 s, respectively. The response values can be seen clearly in Fig. 6b, and the response is nearly linearly proportional to the HCHO concentration in the 0.5–200 ppm range. In 0.5 ppm HCHO, the response value of mesoporous nanoparticles is 4.3. While at 200 ppm formaldehyde, the response value of nanoparticles increased to 222.8. The increase of response was because that removing ZnO phase of the composite material by acid-etching process can leave a large number of smaller pores and defects in the SnO_2 matrix which can improve the surface area of the material and make more active sites to improve the adsorption and exhibit better sensitivity.[2,13,14]

Based on the sensing mechanism, O_2 is primarily physically adsorbed on the surfaces of nanoparticles, and then change to an ionized state at operating temperature, consisting of O^{2-}, O^- and O_2^-. According the response equation:[25,26]

$$R = a \times C^b \quad (1)$$

where R is the response of the material and C is the target gas concentration, a and b are sensitivity parameters and they are constants for a given sensor material, gas and operating temperature. The value of the b is usually 1 for O^- and 0.5 for O^{2-}.[27] As shown in Fig. 6d, the value of b is 0.70 for SnO_2 mesoporous nanoparticles. The value of b is between 0.5 and 1, suggesting that both O^- and O^{2-} oxygen ions at the surface exist at the surface of sensing materials. While $R = 1$, the values of the C are the theoretical minimum detection limit of sensors. The detection limit are 9.8 ppb for sensors based on SnO_2 mesoporous nanoparticles.

Stability and repeatability properties were carried out by operating the sensors at 230 °C. The dynamic response curves of SnO_2 mesoporous nanoparticles within three cycles and the response values within 30 days under the same conditions are

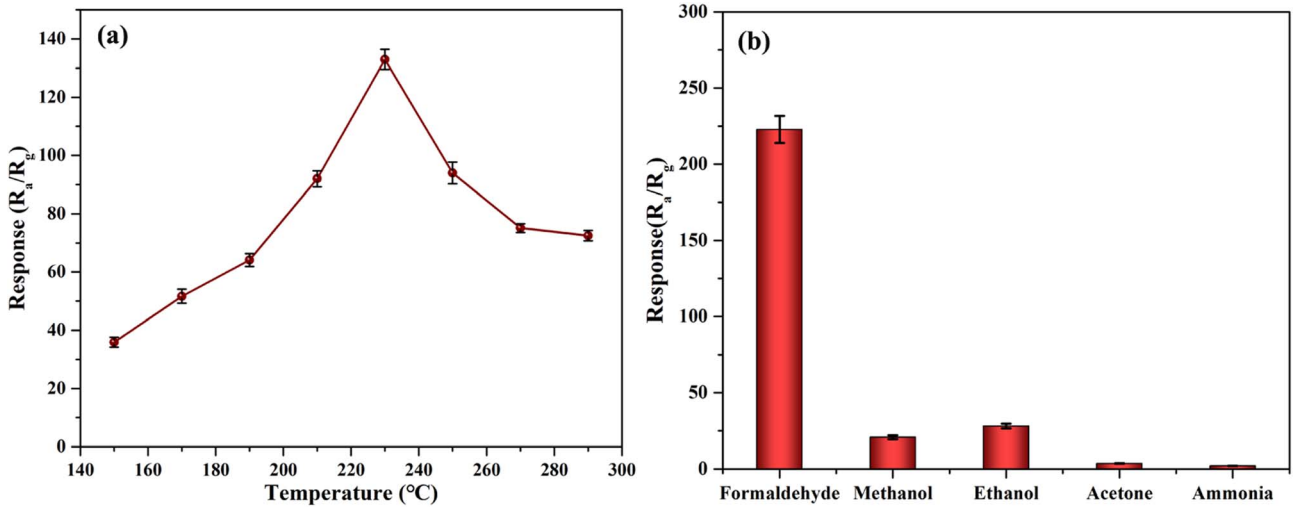

Fig. 5 The response (R_a/R_g) of sensors based on mesoporous nanoparticles. (a) Temperature-dependent sensing responses to 100 ppm HCHO. (b) Selectivity of the sensor to four kinds of interfering gases.

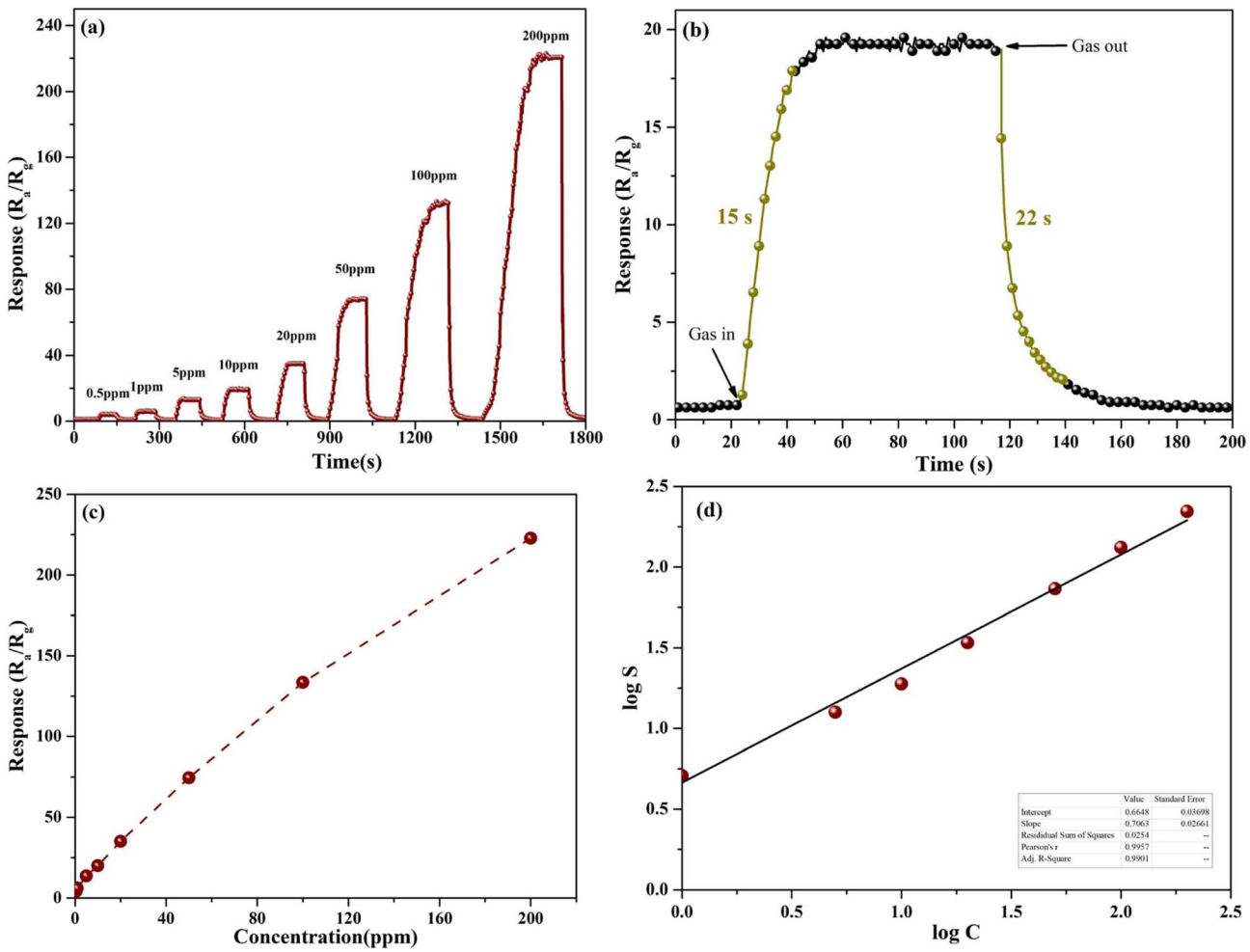

Fig. 6 (a) Real-time HCHO-sensing performance in the concentration range of 0.5 ppm to 200 ppm at 230 °C. (b) Response curves of SnO_2 mesoporous nanoparticles to 10 ppm HCHO. (c) Response values of the sensors to different concentrations of HCHO. (d) The fitting line of log *S* and log *C*.

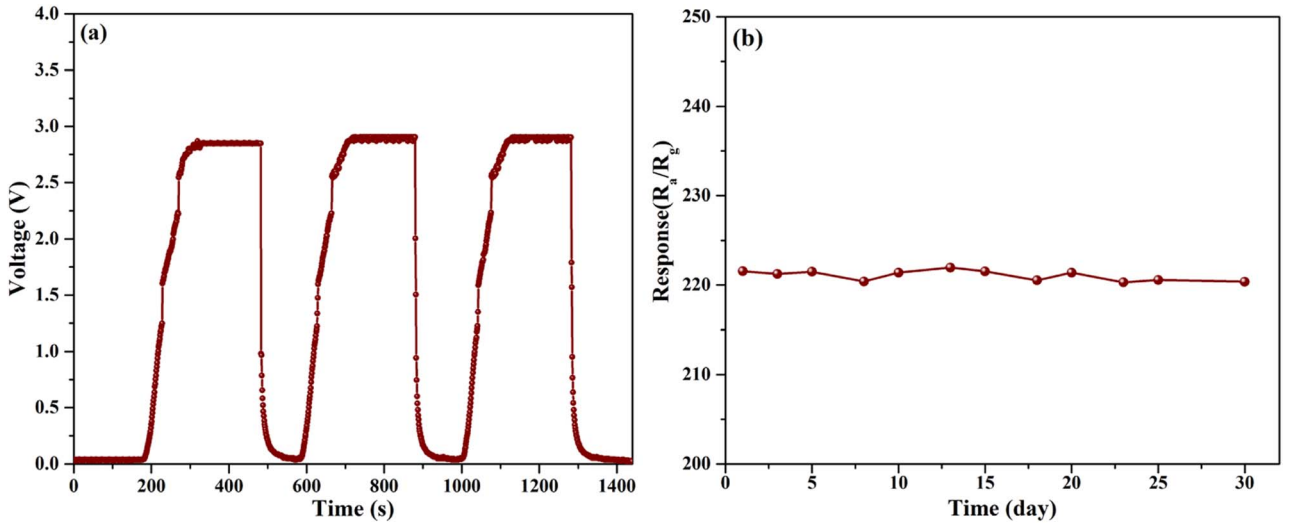

Fig. 7 The dynamic response of sensors based on (a) SnO_2 mesoporous nanoparticles sensor to three cycles of 100 ppm HCHO. (b) Stability tests on the response to 200 ppm of HCHO under the relative 70% humidity environment at 230 °C.

shown in Fig. 7. As can be seen from Fig. 7a, the initial resistance (R_a) of the sample in the air barely changed, and the response value change rate was controlled within 1.9% in all three test cycles. Fig. 7b shows the stability of the response of 200 ppm of HCHO within 30 days. The responses with the 30th cycle show 4.2% decreased compared with the first cycle response for sensors based on SnO_2 mesoporous nanoparticles. The results illustrate the sensor has excellent repeatability and stable performance.

3.3. Gas sensing mechanism

The most widely accepted gas sensitive mechanism is the change in resistance caused by the oxidation–reduction reaction on the metal oxide surface.[9] Specifically, when the gas sensor is exposed to air, oxygen molecules adhere to the surface of the sensing material and capture free electrons from the conduction band to form oxygen ions (O_2^-, O^-, O^{2-}) as shown in eqn (3)–(6), which form electron depletion layer on the surface of nanomaterials. The ionized oxygen species would lead to the increasing of resistance and surface potential barrier ($Ø_a$). The equation can be expressed as follows:

$$O_2(g) \rightarrow O_2(ad) \quad (3)$$

$$O_2(ad) + e^- \rightarrow O^{2-}(ad) \quad (4)$$

$$O^{2-}(ad) + e^- \rightarrow 2O^-(ad) \quad (5)$$

$$O^-(ad) + e^- \rightarrow O^{2-}(ad) \quad (6)$$

When the sensor is placed in the HCHO test gas, they will be attached to the sensor surface, through the oxygen ions above the REDOX reaction, release electrons to the guide band, so the

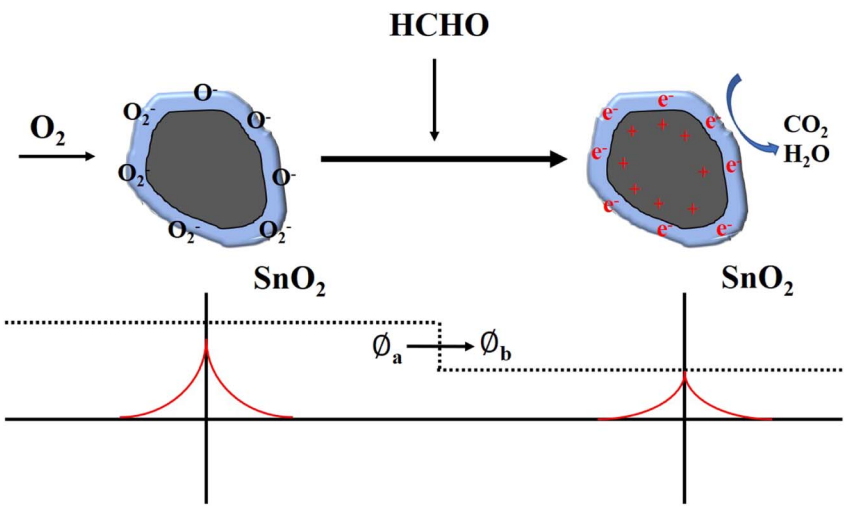

Fig. 8 Schematic diagram of the sensing mechanism of SnO_2 mesoporous nanoparticles.

sensor resistance and surface potential barrier ($Ø_b$) drops. The reaction is as eqn (7) and (8):

$$HCHO(g) + 2O^-(ad) \rightarrow CO_2(g) + H_2O(g) + 2e^- \quad (7)$$

$$HCHO(g) + 2O^{2-}(ad) \rightarrow CO_2(g) + H_2O(g) + 4e^- \quad (8)$$

The surface area and oxygen vacancies are the main reason for the improvement of the gas-sensitive performance of SnO_2 to HCHO as shown in Fig. 8. On one hand, with acid-etching, the specific surface area of the material is improved because acid-etching process can leave a large number of pores in the SnO_2 matrix which can improve the surface area of the material, and more negative oxygen ions can be adsorbed. On the other hand, the accumulation layer of negative oxygen ions is in the hollow inner surface of SnO_2, and the electron depletion layer formed in SnO_2 can reach a deeper position.[13,26] So the sensor based on SnO_2 with acid-etching does not tend to saturate at higher HCHO concentration. The electron depletion layer created by this concave pore structure could even fill the entire grain, because we obtain SnO_2 with the pore diameter region was 2.7–4.5 nm as shown in BET. Furthermore, the mass of oxygen vacancies defects exist with the acid-etching process, which play a very important role in activating oxygen, because it could adsorb oxygen from the gas and weaken its bond to form the activated oxygen species. The increase of amount of oxygen vacancies could produce more activated oxygen species, which could accelerate the oxidation–reduction reaction on the metal oxide surface.[11,26] Therefore, with acid-etching, the resistance change rate of the sample will be improved, and the response will be significantly improved.

4. Conclusion

In summary, this work studied the SnO_2 mesoporous nanoparticles by simple hydrothermal method and took advantage of the difference of solubility of ZnO and SnO_2 in diluted nitric acid to remove ZnO phase. The sensing properties show that the sample exhibites excellent selectivity and response toward HCHO gas due to the higher activities of surface adsorbed oxygen species and the improve of specific surface area. The expansion of electron depletion layer and increasing of oxygen vacancies are considered to be an effect factor to improve the gas sensing performance due to the influence of pore depression surface.[13–15,24–26] In addition, the sensors based on as-prepared mesoporous nanoparticles also exhibited good stability.

Conflicts of interest

There are no conflicts to declare.

Acknowledgements

This work was financially supported by the National Natural Science Foundation of China (11933006, U2141240, 81921002), the Shanghai Innovative Project (2021-cyxt1-kj04), "the Belt and Road" Young Scientist Exchange Program of the Science and Technology Commission of Shanghai (Grant No. 20490743000), Shanghai Natural Science Foundation (Grant No. WF220403061), Oceanic Interdisciplinary Program of Shanghai Jiao.

References

1 S. Muhic and V. Butala, The influence of indoor environment in office buildings on their occupants: expected-unexpected, *Build. Environ.*, 2004, **39**, 289.
2 Y. Y. Xue, J. L. Wang, S. N. Li, Y. C. Jiang, M. C. Hu and Q. G. Zhai, Mesoporous Ag/In_2O_3 composite derived from indium organic framework as high performance formaldehyde sensor, *J. Solid State Chem.*, 2017, **251**, 170.
3 R. Zhang, X. P. Liu, T. T. Zhou and T. Zhang, Controllable construction of multishelled p-type cuprous oxide with enhanced formaldehyde sensing, *J. Colloid Interface Sci.*, 2019, **535**, 58.
4 L. Y. Gai, R. P. Lai, X. H. Dong, X. Wu, Q. T. Luan, J. Wang, H. F. Lin, W. H. Ding, G. L. Wu and W. F. Xie, Recent advances in ethanol gas sensors based on metal oxide semiconductor heterojunctions, *Rare Met.*, 2022, **41**, 1818.
5 Y. Q. Zhang, Y. Y. Liu, L. S. Zhou, D. Y. Liu, F. M. Liu, F. M. Liu, X. S. Liang, X. Yan, Y. Gao and G. Y. Lu, The role of Ce doping in enhancing sensing performance of ZnO-based gas sensor by adjusting the proportion of oxygen species, *Sens. Actuators, B*, 2018, **273**, 991.
6 H. Ji, W. Zeng and Y. Li, Gas sensing mechanisms of metal oxide semiconductors: a focus review, *Nanoscale*, 2019, **11**, 22664.
7 W. Liu, D. Gu, J. W. Zhang, X. G. Li, M. N. Rumyantseva and A. M. Gaskov, ZnSe/NiO heterostructure-based chemiresistive-type sensors for low-concentration NO_2 detection, *Rare Met.*, 2021, **40**, 1632.
8 X. Y. Yao, J. B. Zhao, Z. D. Jin, Z. Jiang, D. M. Xu, F. L. Wang, X. M. Zhang, H. X. Song, D. Pan, Y. X. Chen, R. B. Wei, Z. H. Guo, J. R. Liu, N. Naik, R. T. Wang and L. L. Wu, Flower-like hydroxyfluoride-sensing platform toward NO_2 detection, *ACS Appl. Mater. Interfaces*, 2021, **12**, 26278–26288.
9 H. Hashtroudi, I. D. Machinnon and M. Shafiei, Emerging 2D hybrid nanomaterials: towards enhanced sensitive and selective conductometric gas sensors at room temperature, *J. Mater. Chem. C*, 2020, **8**, 13108–13126.
10 X. Song, Q. Xu, T. Zhang, B. Song, C. C. Li and B. Q. Cao, Room-temperature, high selectivity and low-ppm-level triethylamine sensor assembled with Au decahedrons-decorated porous α-Fe_2O_3 nanorods directly grown on flat substrate, *Sens. Actuators, B*, 2018, **268**, 170.
11 T. T. Yu, X. L. Cheng, X. F. Zhang, L. L. Sui, Y. M. Xu, S. Gao, H. Zhao and L. H. Huo, Highly sensitive H_2S detection sensors at low temperature based on hierarchically structured NiO porous nanowall arrays, *J. Mater. Chem. A*, 2015, **3**, 11991.
12 S. Y. Liu, L. Teng, Y. Zhao, Z. Liu, J. W. Zhang, M. Ikram, A. U. Rehman, L. Li and K. Shi, Facile route to synthesize porous hierarchical Co_3O_4/CuO nanosheets with high

porosity and excellent NO_x sensing properties at room temperature, *Appl. Surf. Sci.*, 2018, **450**, 91.

13 W. Zhang, X. Cheng, X. Zhang, Y. Xu, S. Gao, H. Zhao and L. Huo, High selectivity to ppb-level HCHO sensor based on mesoporous tubular SnO_2 at low temperature, *Sens. Actuators, B*, 2017, **247**, 664–672.

14 S. Tian, X. Ding, D. Zeng, J. Wu, S. Zhang and C. Xie, A low temperature gas sensor based on Pd-functionalized mesoporous SnO_2 fibers for detecting trace formaldehyde, *RSC Adv.*, 2013, **3**, 11823–11831.

15 H. Y. Yuan, S. A. A. Aljneibi, J. R. Yuan, Y. X. Wang, H. Liu, J. Fang, C. H. Tang, X. H. Yan, H. Cai, Y. D. Gu, S. J. Pennycook, J. F. Tao and D. Zhao, ZnO nanosheets abundant in oxygen vacancies derived from metal-organic frameworks for ppb-level gas sensing, *Adv. Mater.*, 2019, **31**, 1807161–1807169.

16 H. Wang, Y. Qu, H. Chen, Z. Lin and K. Dai, Highly selective *n*-butanol gas sensor based on mesoporous SnO_2 prepared with hydrothermal treatment, *Sens. Actuators, B*, 2014, **201**, 153.

17 N. Devabharathi, A. M. Umarji and S. Dasgupta, Fully inkjet-printed mesoporous SnO_2-based ultrasensitive gas sensors for trace amount NO_2 detection, *ACS Appl. Mater. Interfaces*, 2020, **12**, 57207.

18 X. Y. Xiao, L. L. Liu, J. H. Ma, Y. Ren, X. W. Cheng, Y. H. Zhu, D. Y. Zhao, A. A. Elzatahry, A. Alghamdi and Y. H. Deng, Ordered mesoporous tin oxide semiconductors with large pores and crystallized walls for high-performance gas sensing, *ACS Appl. Mater. Interfaces*, 2018, **10**, 1871.

19 J. H. Ma, Y. Ren, X. R. Zhou, L. L. Liu, Y. H. Zhu, X. W. Cheng, P. C. Xu, X. X. Li, Y. H. Deng and D. Y. Zhao, Pt nanoparticles sensitized ordered mesoporous WO_3 semiconductor: gas sensing performance and mechanism study, *Adv. Funct. Mater.*, 2018, **28**, 1705268.

20 Y. J. Jeong, W. T. Koo, J. S. Jang, D. H. Kim, M. H. Kim and I. D. Kim, Nanoscale PtO_2 catalysts-loaded SnO_2 multichannel nanofibers toward highly sensitive acetone sensor, *ACS Appl. Mater. Interfaces*, 2018, **10**, 2016.

21 F. Zheng, L. Zhang, Y. Y. Li, Q. C. Liu, Z. J. Lim and H. C. Yao, Bimetallic AuPd alloy nanoparticles decorated on macroporous WO_3 supports for selective detection of acetone, *ACS Appl. Nano Mater.*, 2021, **4**, 2713.

22 Y. Qu, H. Wang and H. Chen, Synthesis, characterization and sensing properties of mesoporous C/SnO_2 nanocomposite, *Sens. Actuators, B*, 2016, **228**, 595.

23 R. K. Brow, An XPS study of oxygen bonding in zinc phosphate and zinc borophosphate glasses, *J. Non-Cryst. Solids*, 1996, **194**, 267.

24 J. X. Zhang, F. Lv, Z. H. Li, G. Y. Jiang, M. J. Tan, M. L. Yuan, Q. H. Zhang, Y. P. Cao, H. Y. Zheng, L. L. Zhang, C. Tang, W. Y. Fu, C. Liu, K. H. Liu, L. Gu, J. K. Jiang, G. J. Zhang and S. J. Guo, Cr-doped Pd metallene endows a practical formaldehyde sensor new limit and high selectivity, *Adv. Mater.*, 2022, **34**, 2105276.

25 D. Wang, L. Tian, H. J. Li, K. Wan, X. Yu, P. Wang, A. Y. Chen, X. Y. Wang and J. H. Yang, Mesoporous ultrathin SnO_2 nanosheets *in situ* modified by graphene oxide for extraordinary formaldehyde detection at low temperatures, *ACS Appl. Mater. Interfaces*, 2019, **11**, 12808–12818.

26 H. Hashtroudi, P. Atkin, I. D. R. Mackinnon and M. Shafiei, Low-operating temperature resistive nanostructured hydrogen sensors, *Int. J. Hydrogen Energy*, 2019, **44**, 26646–26664.

27 L. X. Zhang, J. H. Zhao, J. F. Zheng, L. Li and Z. P. Zhu, Hydrothermal synthesis of hierarchical nanoparticle-decorated ZnO microdisks and the structure-enhanced acetylene sensing properties at high temperatures, *Sens. Actuators, B*, 2011, **158**, 144.